Egypt. J. Chem. **Vol. 66,** No. SI 13 pp. 2013 - 2031 (2023)

Egyptian Journal of Chemistry

http://ejchem.journals.ekb.eg/

Empirical and Computational Investigation of Cationic Gemini Surfactants as Anti-Corrosive Inhibitors for Mild Steel in Acid Medium and its silver Nano Structure synthesis and Analysis.

Muhammad G. Gaballah [a,b], Mahmoud A. Bedair [a,c], Ahmed H. EL-Ged[d*] , Samir A. Soliman [a], Emad A. Badr [d*], Moustafa F. Bakr [a]

a Department of Chemistry, Faculty of Science (Men's Campus), Al-Azhar University, Nasr City 11884, Cairo, Egypt.

b Suez Methanol Derivatives Company, Egyptian Ministry of Petroleum and Mineral Resources, Egypt.

c College of Science and arts, University of Bisha, Al-Namas 61977, P.O. Box 101, Saudi Arabia.

d Petrochemical Department, Egyptian Petroleum Research Institute, Egypt.

Abstract

Cationic geminies play an important role nowadays in many industrial applications concerned in protection of eco system (corrosion resistance). The three cationic Gemini surfactants based on amide of succinic acid (OGC, DGC, HGC) were evaluated as anti-corrosive materials for mild steel (MS) in 0.5 mol/L H_2SO_4 medium. The inhibition efficiencies were evaluated using gravimetric, electrochemical techniques, and computational approaches. The findings showed that HGC was the most effective inhibitor, with an efficacy of 95.25% at $1x10^{-3}$ M using EIS measurements. The inhibitors were found to form protective layers on the MS surface, as indicated by modifications in impedance parameters (C_{dl}, double layer capacitance, and R_{ct}, charge transfer resistance). Thermodynamic and kinetic parameters of adsorption were estimated to elucidate the inhibitive mechanism. AFM images revealed a smoother surface of MS and less corroded area in the presence of the investigated inhibitors compared to their absence. Also this study describes the synthesis of silver Nano particles capped surfactant. Silver Nano structures were characterized using DLS and TEM images.

Overall, the study highlights the potential of these Gemini surfactants as anti-corrosive materials for mild steel. And stabilizers for preparing silver Nano particles capped surfactants.

Keywords : cationic geminin surfactants; Atomic force microscope; Monte Carlo simulations; silver Nano particles.

1. Introduction

In the petrochemical, chemical, thermal, nuclear power, and other industries, steel metal and its alloys are frequently utilized as a significant portion of construction materials **[1]**. For pickling purposes, acid solutions like HCl and H_2SO_4 are frequently utilized to eliminate rust and scale off the surface of MS **[2]**. However, the metal corrodes unintentionally as a result of the acid cleaning process. Despite the fact that MS is extensively utilized in many sectors as a result of its various physical and mechanical properties, its corrosion in mineral acids e.g., H_2SO_4 represents an extreme depletion of both money and assets **[3]** as well as corrosion engineers and specialists regard MS corrosion to be one of the dangerous issues they must deal with **[4]**. Reduction in metals deterioration can be achieved using different techniques, such as alloying, coating, materials modernizing, environment cleansing and inhibitors. However, the utilizing of inhibitors as anticorrosion is regarded as the most efficient way for preserving metals and alloys against corrosion and environmental conditions in a variety of industries **[5, 6]** because its affordability and simplicity of use **[7, 8]**. The substances whose chemical structure include heteroatoms as well as π electrons are properly known as acid inhibitors. These centers facilitate the inhibitor adsorption onto metal surface which minimizing the corrosion rate by obstructing the active sites **[9, 10]**. Surfactants play an crucial role in corrosion inhibitor production and which are used for aggressive media like acid and salty media due to their low cost and high efficiency **[11]**.

Gemini surfactant is made up of two regular surfactant molecules joined chemically by a spacer chain and which has various features such as low cost, low toxicity and high surface activity **[12]**. Cationic

*Corresponding author e-mail: emadabadr@yahoo.com.; ahmedelged2010@yahoo.com.

Receive Date: 13 July 2023, Revise Date: 12 August 2023, Accept Date: 23 August 2023

DOI: 10.21608/EJCHEM.2023.222841.8256

Gemini Surfactants that poses a significant adsorptive feature at the metal surface because of their chemical structure as well as their electronegative atoms are widely utilized as metals corrosion inhibitors, especially in acidic media.**[13, 14]**. The conventional amide surfactant was explored as a corrosion inhibitor for mild steel in acidic medium. The formulated particles primarily comprise environmentally friendly components such as palmitic acid and amine. These components exhibit effective inhibition characteristics in acidic environments. As a result, the Gemini amide surfactant demonstrated significant efficacy in safeguarding mild steel from corrosion, while also being environmentally benign**[15].** metallic nanoparticles, like gold, and silver nanoparticles, have gained significant attention due to their reactivity and selectivity in many fields such as catalytic degradation of organic pollutants. Silver nanoparticles, in particular, are widely used as catalysts for reducing organic dyes due to their abundance and cost-effectiveness. However, Silver nanoparticles are susceptible to oxidation and have a tendency to agglomerate together**[16, 17]**. Many methods are employed to stabilize produced nanoparticles, and one of the most cost-effective and efficient approaches is green synthesis, which utilizes surfactants as capping agents**[18]**.

Our current study's goal is to create and assess the inhibition impact of the investigated OGC, DGC and HGC inhibitors on MS corrosion submerged in 0.5 mol/L H_2SO_4 media utilizing gravimetric, electrochemical techniques and computational approaches. Kinetic and thermodynamic parameters along with these inhibitors' adsorption mechanism onto MS surface are discussed. Using the surfactant in our study in green synthesis of silver Nano structures and stabilization of it.

2. Materials and experimental techniques

2.1. materials

All chemicals were of high purity and were used exactly as they were supplied. N^1, N^1-dimethylethane-1,2-diamine, succinic acid, 1-bromooctane, 1-bromododecane, and 1-bromohexadecane were purchased from Sigma-Aldrich. Throughout, deionized water was used. Silver nitrate were purchased from sigma Aldrich. All solvents were purchased from Al - Gomhoria chemical company and they are utilized as received.

2.2. Material Preparation

2.2.1. preparation of cationic Gemini surfactant

the three surfactant were prepared according to previous work[19] 2 mole of N1,N1-dimethylethane-1,2-diamine and 1 mole of succinic acid were mixed in xylene at 140 ^oC using (PTS) as a catalyst N1,N4-bis(2-(dimethylamino)ethyl) succinamide. Were obtained after washing by petroleum ether the product refluxed with 1-bromooctane, 1-bromododecane and 1-bromohexadecane in 100 ml ethanol to obtain the targeted surfactant OGC , DGC and HGC respectively

2.2.2. preparation of surfactant capped silver Nano particles

A green synthesis method was employed to prepare OGC/Ag Nano, DGC/Ag Nano, and HGC/Ag Nano by mixing equal amounts of surfactant aqueous solution (5×10^{-3}M) and silver nitrate solution (5×10^{-3}M) and exposing the mixture to sunlight for 7 minutes until a noticeable change in the colour of the solution was observed.**[20, 21]**.

2.2.3. Utilizing coupon

The sheets utilized for this investigation are mild steel sheets, MS, possess the composition; Mo (0.01 wt.%), Mn (1.35 wt.%), Ni (0.02 wt.%), S (0.01 wt.%), Cr (0.05 wt.%), Si (0.22 wt.%), P (0.017 wt.%), C (0.23 wt.%), and Fe (98.093 wt.%). MS sheets with total surface area 46.8 cm^2 were gradually abraded using various emery papers grades then degreased using acetone then rinsed by distilled water and finally dried.

2.3. Experimental techniques

2.3.1. Weight loss technique:

The utilized coupons precisely weighted, MS sheets were submerged in 100 ml of H_2SO_4 medium for 24 h at 25, 45 and 65 °C in the existence along with lack of OGC, DGC and HGC inhibitors at different concentrations. Then, these sheets were taken off, cleaned using distilled water, acetone, and then dried, reweighed precisely after being scrubbed under running water using a bristle brush to eliminate the corrosion products. The MS specimens did indeed lose weight. For the highest level of reproducibility, each experiment was executed in three duplicates. Three parallel sheets that were taken into consideration had their average weight loss values estimated.

2.3.2. Electrochemical techniques

All electrochemical experiments were performed in a three electrode cylindrical glass cell with a Volta lab 40 PGZ-301, in which the prepared MS electrode served as the working electrode, WE, while the saturated calomel electrode, SCE, served as the reference electrode, RE, and the platinum electrode served as the counter electrode, CE, and electrolyte media were 0.5 mol/L H_2SO_4 media without or with the synthesized Gemini inhibitors at various concentrations. Before beginning the measurements, the WE was handled as in a weight loss experiment and placed in the tested solution for an hour. 0.7 cm^2 of the electrode was the unprotected part subjected to the corrosive solution. The temperature for all experiments was 25 ^oC. Potentiodynamic polarization measurements (PDP) were done by automatically altering the electrode potential at open circuit potential (OCP) from -1000 mV to -200 mV against the

saturated calomel electrode) with 2 mV/s scan rate. For the electrochemical impedance measurements, the excitation signal at open circuit potential was 4 mV sine wave, and the frequency adjusted from 100 kHz to 50 mHz.

Table 1. Corrosion rate, surface coverage and percentage inhibition efficiency of MS in 0.5 M H_2SO_4 of the synthesized Gemini Surfactants inhibitors (OGC, DGC, HGC) at different temperatures

Inhibitor	Inhibitor Conc. (M)	25ºC			45ºC			65ºC		
		K_{corr} (mg cm^{-2} h^{-1})	θ	η_w(%)	K_{corr} (mg cm^{-2} h^{-1})	θ	η_w(%)	K_{corr} (mg cm^{-2} h^{-1})	θ	η_w(%)
Blank		1.438	…...	…...	2.271	…...	…...	3.259	…...	…...
OGC	1.00×10^{-5}	0.790	0.450	45.04	1.153	0.492	49.22	1.576	0.516	51.64
	5.00×10^{-5}	0.600	0.583	58.26	0.841	0.630	62.96	1.117	0.657	65.73
	1.00×10^{-4}	0.505	0.649	64.89	0.687	0.697	69.74	0.911	0.721	72.06
	5.00×10^{-4}	0.437	0.696	69.61	0.570	0.749	74.91	0.716	0.780	78.02
	1.00×10^{-3}	0.338	0.765	76.51	0.434	0.809	80.90	0.534	0.836	83.62
DGC	1.00×10^{-5}	0.760	0.471	47.15	1.086	0.522	52.19	1.472	0.548	54.83
	5.00×10^{-5}	0.538	0.626	62.60	0.747	0.671	67.11	0.971	0.702	70.21
	1.00×10^{-4}	0.437	0.696	69.62	0.588	0.741	74.10	0.744	0.772	77.18
	5.00×10^{-4}	0.358	0.751	75.12	0.467	0.794	79.44	0.574	0.824	82.38
	1.00×10^{-3}	0.285	0.802	80.21	0.360	0.842	84.16	0.435	0.867	86.65
HGC	1.00×10^{-5}	0.675	0.531	53.06	0.950	0.582	58.16	1.267	0.611	61.14
	5.00×10^{-5}	0.509	0.646	64.63	0.628	0.724	72.35	0.750	0.770	77.00
	1.00×10^{-4}	0.409	0.716	71.57	0.468	0.794	79.41	0.530	0.837	83.75
	5.00×10^{-4}	0.328	0.772	77.16	0.359	0.842	84.20	0.391	0.880	88.00
	1.00×10^{-3}	0.231	0.839	83.90	0.252	0.889	88.90	0.273	0.916	91.62

Table 2. Activation parameters for MS in 0.5 M H_2SO_4 in the absence and presence of different concentration of the synthesized Gemini Surfactants inhibitors (OGC, DGC, HGC)

Inhibitor	Conc.Of inhibitor (M)	Ea (kJ/mol)	ΔH* (KJ/mol)	ΔS* (J/mol k)
Blank	**…....**	**17.15**	**14.52**	**-193.113**
OGC	1.00×10^{-5}	14.46	11.83	-207.14
	5.00×10^{-5}	13.01	10.38	-214.30
	1.00×10^{-4}	12.34	9.71	-218.01
	5.00×10^{-4}	10.35	7.71	-225.89
	1.00×10^{-3}	9.58	6.95	-230.58
DGC	1.00×10^{-5}	13.85	11.21	-209.53
	5.00×10^{-5}	12.38	9.74	-217.32
	1.00×10^{-4}	11.15	8.52	-223.16
	5.00×10^{-4}	9.92	7.29	-228.94
	1.00×10^{-3}	8.89	6.25	-234.34
HGC	1.00×10^{-5}	13.19	10.55	-212.74
	5.00×10^{-5}	8.13	5.49	-232.08
	1.00×10^{-4}	5.42	2.78	-243.01
	5.00×10^{-4}	3.66	1.02	-250.73
	1.00×10^{-3}	3.47	0.83	-254.27

2.3.3. Morphological study of the metal surface

AFM images were conducted via Nano-surf C3000 instrument to assess the roughness of surface and provide 3 D image of MS after submersion in a corrosive medium in the existence along with lack of the synthesized Gemini inhibitors for 24 h.

2.3.4. Quantum Chemical (QC) calculations

To further support the experimental results, Quantum Chemical (QC) calculations Monte Carlo (MC) simulations have been performed. Computational calculations were done by Dmol3 and adsorption locator modules incorporated into the Biovia Materials studio program. The geometry optimization using Dmol3 included the LDA/ PWC / DN (4.4) and COSMO for solvent. The surfactants molecule's interaction with MS surfaces (least closely stacked plane) were done using a simulation box (27.31 Å 40.54 Å 58.42 Å) with periodic boundary variables. A 10-layer slab model was used for modeling the surface of MS, where each layer represented a (10 x 20) unit cell. For the solvent we used, 300 H_2O, 20 H_3O^+, and 10 SO_4^{--} molecules.

2.3.5. Studying the silver Nano structures

The prepared silver Nano structures were studied using Dynamic Light Scattering (DLS) instrument (Malvern Zeta sizer Nano device, Nano Series (HT), Nano ZS, Worcestershire, UK at EPRI) . DLS was applied to determine whether the prepared silver nanostructures in the Nano size or not and zeta potential, as well.

The particle morphologies of OGC/AgNPs, DGC/AgNPs, and HGC/AgNPs were investigated using a Joel JeM-2100 Transmission Electron Microscope (TEM) (Japan) at EPRI. TEM was also used to affirm the size and distribution of the prepared nanoparticles.

3. Results and discussion

3.1. Corrosion and Kinetic measurements

3.1.1. Concentration impact

The current investigation assessed the influence of the synthesized inhibitors under consideration as anticorrosion for MS submerged in a medium of 0.5 mol/L of H_2SO_4 at 25, 45, 65 °C for 24 h in both the existence and lack of these inhibitors at ($1.0x10^{-5}$ – $1x10^{-3}$) M. The rate of corrosion, K_{corr}, (mg/cm^2 h), can be evaluated as below:

$$K_{corr} = \frac{\Delta W}{At} \quad (1)$$

as weight loss of the specimen, ΔW, the total initial surface area of the specimen, A, and immersion time, t. The surface coverage degree (θ) was estimated by equation (2):

$$\theta = 1 - \frac{\Delta W_i}{\Delta W_o} \quad (2)$$

where, ΔW_i represent the steel specimen weight losses in the existence of inhibitors and ΔW_o (mg) represent the steel specimen weight losses in the lack of inhibitors. Besides, we can obtain the inhibition efficiency, η_w % by:

$$\eta_w\% = \theta \text{ x } 100 \quad (3)$$

Table (1) scheduled the obtained data which revealed the corrosion rates, K_{corr}, decrease by rising the concentrations of synthesized inhibitors as a consequence of reducing the steel weight loss which may arise from increasing the synthesized inhibitors' adsorption onto MS surface raising its surface coverage degree, θ, and inhibition efficacy, η_w %. Undoubtedly, this inhibitor adsorption process can form a protective film onto MS surface diminishing the interaction between the aggressive medium and the surface of MS. Hence, the aggressive environment impact on the MS surface will be minimized. Consequently, this adsorption may attributed to the electrostatic interaction between the surface of MS and the cationic Gemini surfactants inhibitors **[22]**.

3.1.2. Temperature impact

Herein, the temperature impact on the inhibition efficacy of OGC, DGC and HGC inhibitors on MS corrosion in a medium of 0.5 mol/L of H_2SO_4 was inspected. Table (1) provides clarification that the corrosion rate increases with the elevation of medium temperature within the range of 25°C to 65°C. This phenomenon is attributed to the accelerated transfer of aggressive ions at higher temperatures.

Furthermore, the inhibition provided by the synthesized inhibitors demonstrates an upward trend as the temperature increases. This trend suggests a robust adsorption (chemisorption) of the inhibitors onto the steel surface, leading to molecular-level chemical modifications. Consequently, this process enhances the electron densities of the active centers within the Gemini inhibitors, consequently promoting a more substantial adsorption effect. As a result, the corrosion inhibition efficacy experiences an enhancement. **[23]**.

To evaluate the energy of activation, Ea, in relation to corrosion, we apply the Arrhenius equation shown below:

$$ln\mathrm{K} = (-\mathrm{E_a}/\mathrm{RT}) + ln\mathrm{A} \quad (4)$$

Where the corrosion rate, k, the universal gas constant, R, Arrhenius coefficient, A, and kelvin temperature, T.

The ln k against 1/T plots in the existence along with lack of the regarded inhibitors at different concentrations are depicted in Fig. 1A by which the E_a can be determined from the slope ($-E_a$ /R) as listed in Table (2) in which the E_a values in the lack of the inhibitors are higher than E_a values in the existence of

it. Their reduced values are attributed to chemical adsorption of our inhibitors onto MS surface [24].

In the light of the transition state theory, the change in activation parameters (ΔH*, ΔS*) can be extracted by the following Wine-Jones-Erying equation:

$$K_{corr} = {RT}/{Nh}\ exp^{\left({\Delta S^*}/{R}\right)}\ exp^{\left({-\Delta H^*}/{RT}\right)} \quad (5)$$

Where h represents Plank's constant, R represents universal gas constant, and N represents Avogadro's number. Straight lines are given from ln (k/T) against 1/T plot in the existence along with lack of these inhibitors at the studied concentrations as represented in **Fig. 1B**, with an intercept of (ln (R./Nh) + ΔS*/R) and a slope of (-ΔH*/R). The ΔH* and ΔS* values are evaluated and reported in **Table (2).**

The ΔH* and ΔS* values in existence of the inhibitors are lower than those in their lack of. The positive ΔH* values reveal the endothermicity and the difficulty of MS corrosion dissolution process in existence of the Gemini inhibitors **[25]**.

Furthermore, the negative values of ΔS* in the existence along with lack of these inhibitors emphasize that in the rate determining stage, the activation complex is an association instead of dissociation referring to more ordering that occurs when moving from reactant species to activated complex by constituting a stable adsorption film onto MS surface from the inhibitors' molecules **[26]**.

3.2. Adsorption isotherm

The inhibitors molecule's molecular interactions with MS surface active sites are depicted using the adsorption isotherms. The surface coverage degree, θ, values fit the different adsorption isotherms while by the correlation coefficient (R^2), the adsorption isotherm model can be chosen to well fit the experimental results and hence Langmuir isotherm model was applied to our study

$$C/\theta = C + (1/K_{ads}) \quad (6)$$

where the equilibrium constant, K_{ads}, and inhibitor concentration, C. The C / θ vs. C linear relationship, which indicated in **Fig. 2**, suggests that these synthesized Gemini inhibitor's adsorptions onto MS surface compiled with Langmuir's adsorption isotherm and the obtained correlation coefficient (R^2) of this isotherm is being almost unity as listed in **Table (3)**.

However, the obtained straight lines slopes from the Langmuir isotherm plots for these inhibitors are greater than unity, referring each inhibitor unit occupies greater than one adsorption active center. Hence, the adsorption process at certain temperature can be more convenient to be employed using Villamil isotherm (modified Langmuir equation) as below **[27]**:

$$C/\theta = nC + (n/K_{ads}) \quad (7)$$

where, slope, n, represents the quantity of adsorbed H_2O molecules that were displaced from MS surface whereas the intercept enables for the determination of the equilibrium constant K_{ads} for the inhibitors under study as cited in **Table (3)**.

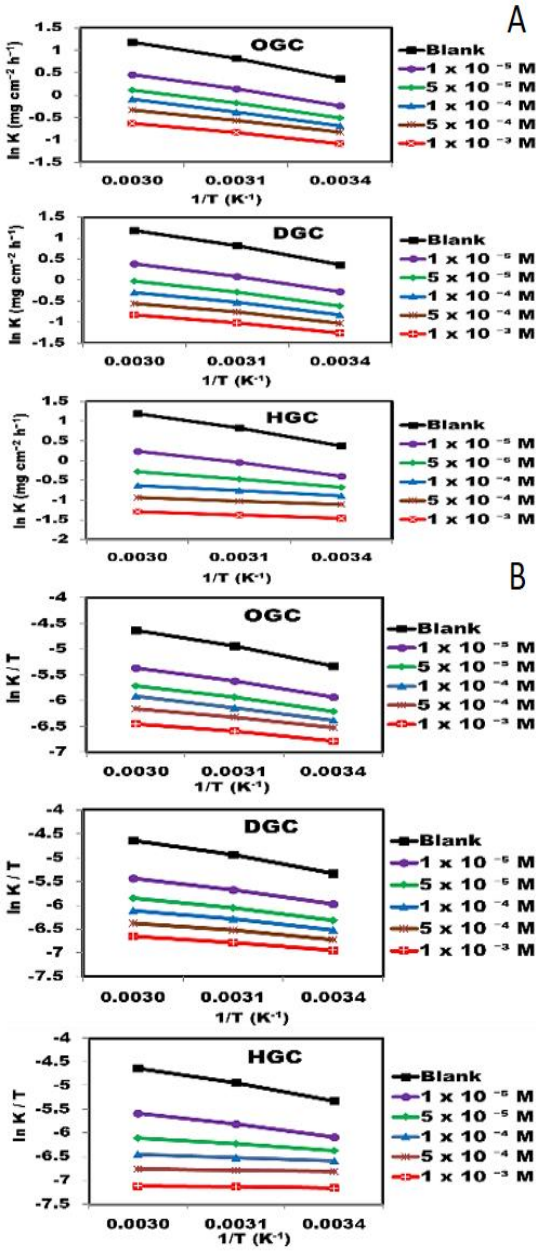

Figure 1: (A) Arrhenius plots of ln k vs. 1/T for MS in 0.5 M H_2SO_4; **(B)** A plot of ln k /T vs. 1/T for MS in 0.5 M H_2SO_4 in the absence and presence of the synthesized cationic surfactants inhibitors (OGC, DGC, HGC) with different concentrations.

Table 3. Thermodynamic parameters from Villamil adsorption isotherm of MS in 0.5 M H_2SO_4 in the presence of different concentration of the synthesized Gemini Surfactants inhibitors (OGC, DGC, HGC) at different temperatures.

Inhibitor	Temp (K)	Slope	R^2	K_{ads} (M^{-1})	ΔG^o_{ads} (kJ/mol)	ΔS^o_{ads} (J/mol.K)	ΔH^o_{ads} (kJ/mol)
OGC	298	1.3026	0.9980	39916.23	-36.20	140.647	5.713
	318	1.2307	0.9987	48179.11	-39.13	141.006	
	338	1.1903	0.9990	52343.86	-41.82	140.632	
DGC	298	1.2398	0.9991	50292.76	-36.77	143.776	6.073
	318	1.1816	0.9993	59088.87	-39.67	143.834	
	338	1.1475	0.9995	67198.37	-42.52	143.774	
HGC	298	1.1872	0.9984	47786.18	-36.65	166.832	13.070
	318	1.1201	0.9994	69954.45	-40.11	167.242	
	338	1.0870	0.9997	89027.6	-43.31	166.814	

It is worthy that thermodynamic functions of adsorption process are crucial for the prediction of the adsorption mechanism onto MS surface. Van't Hoff formula can be employed to estimate the change in standard adsorption enthalpy (ΔH^o_{ads}).

$$ln K_{ads} = -\Delta H^o_{ads}/(RT) + \text{Constant} \qquad (8)$$

The standard adsorption free energy change (ΔG^o_{ads}) as well as the standard adsorption entropy change (ΔS^o_{ads}) can be estimated by equations (9, 10):

$$\Delta G^o_{ads} = -RTLn(55.5K_{ads}). \qquad (9)$$

Where, the water molarity (mol/l) in the solution is 55.5.

$$\Delta S^o_{ads} = (\Delta H^o_{ads} - \Delta G^o_{ads})/T. \qquad (10)$$

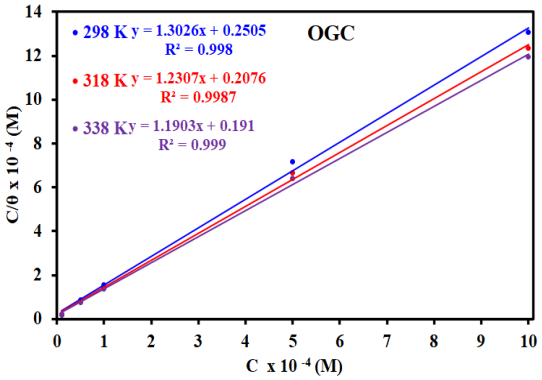

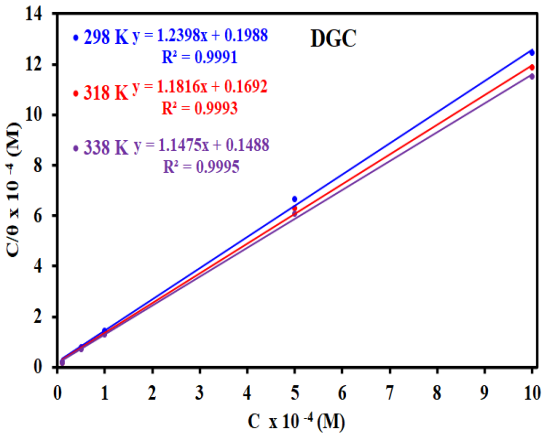

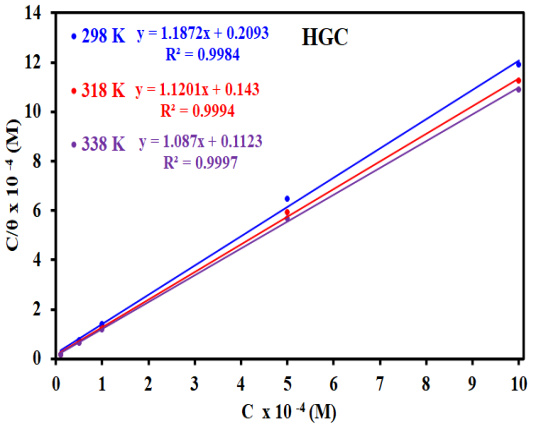

Figure 2: Villamil adsorption isotherm of the MS in 0.5 M H_2SO_4 in the presence of the synthesized cationic surfactants inhibitors (OGC, DGC, HGC) with different concentrations.

The findings are cited in **Table (3)** where the positive ΔH^o_{ads} values revealed endothermic adsorption process of the inhibitors (OGC, DGC, HGC) and indicates the difficulty of MS dissolution interpreting a rise in the efficiency of inhibition as the temperature rises which results in sorption of the

inhibitors molecules onto MS surface. As a result, the efficiency of inhibition will increase. The negative ΔG^{o}_{ads} (-36.20 to -43.31 kj mol^{-1}) values reveal the process of adsorption is a mixture of physical and chemical adsorption with a predominance of chemisorption **[28]** and also indicate spontaneous adsorption process of the inhibitors onto the MS surface as depicted in **Table (3)**. In addition, the positive ΔS^{o}_{ads} values cited in **Table (3)** clarifies that the entropy always increases throughout endothermic adsorption process, which controls the adsorption of the OGC, DGC and HGC inhibitors onto the surface of MS **[29]**.

3.3. Electrochemical-techniques

3.3.1. Potentiodynamic-polarization measurements (PDP)

In this study, the polarization data of MS in a medium of 0.5 mol/L of H_2SO_4 without and with OGC, DGC and HGC inhibitors at the considered concentrations were illustrated in **Fig.3**. The extracted various electrochemical corrosion parameters can be donated via extrapolation of Tafel curves with efficiency of inhibition, η_{pdp} %, and surface coverage area, θ, as collected in **Table (4)**.

The efficacy of inhibition, η_{pdp} %, and the surface. coverage degree, θ, are evaluated as follows:

$$\theta = 1 - (\frac{I}{I_o}) \qquad (12)$$

$$\eta_{pdp}\,\% = \left(1 - \left(\frac{I}{I_o}\right)\right) \times 100 \qquad (13)$$

as I represent the corrosion current densities in existence of the investigated inhibitors, and I_o represents the corrosion current densities in lack of the investigated inhibitors.

Table (4) reveals a diminish in corrosion current density, $i_{corr.}$, by raising the inhibitors' concentrations, and η_{pdp} % increases due to increasing the blocked fraction by inhibitors' adsorption onto the electrode surface as well, and hence θ increases.**[30, 31]**

Not only OGC, DGC and HGC inhibitors affect both the cathodic and anodic reactions but also upon increasing their concentrations, they don't alter the inhibitive reaction mechanism **[32]**. All of this arise from the slight change of Tafel slopes (βa) and (βc) of these inhibitors.

As presented in **Table (4)**, corrosion potential values, E_{corr}, are shifted towards the negative by inhibitors addition. Given that the highest shift at 25 °C does not surpass 85 mV (vs. SCE), it can be expected that OGC, DGC and HGC inhibitors belong in the category of mixed type (anodic/cathodic) inhibitors, which diminish the anodic dissolution of MS while simultaneously delays the cathodic hydrogen evolution reaction **[33]**.

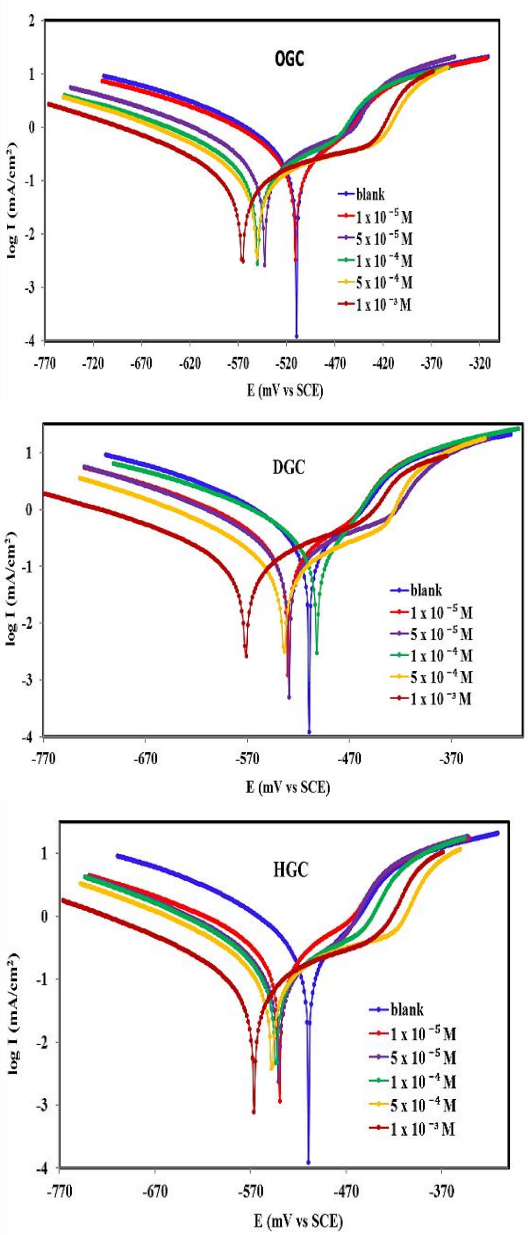

Figure 3: Potentiodynamic polarization curves for the corrosion of MS in 0.5 M H_2SO_4 in the absence and presence of the synthesized cationic surfactants inhibitors (OGC, DGC, HGC) with different concentrations.

3.3.2. Electrochemical impedance spectroscopy

Besides, another reliable and an important technique is the electrochemical impedance spectroscopy (EIS) which gives kinetic data regarding steel/medium interface that displays steel corrosion. As seen in **Figs 4 (A, B)** the Nyquist plots and Bode and phase angle plots for MS immersed in a medium of 0.5 mole/L of H_2SO_4 in the existence along with lack of the synthesized cationic Gemini surfactants' inhibitors (OGC, DGC, HGC) at the considered concentrations.

Table 4. Electrochemical parameters for MS dissolution in 0.5 M H_2SO_4 solution containing different concentrations of the OGC, DGC and HGC inhibitors obtained from polarization measurements at 25 °C.

Inhibitor	Conc. (M)	E_{corr} vs.SCE (mV)	I_{corr} (μA cm^{-2})	β_a (mV dec^{-1})	β_c (mV dec^{-})	k (mm/y)	θ	η_p%
Blank	--------	-509.5	1108.7	123.3	-216.5	12.96	-----	-----
OGC	1.00×10^{-5}	-510.7	720.1	108.0	-192.7	8.422	0.3505	35.05
	5.00×10^{-5}	-542.8	534.1	112.7	-194.0	6.247	0.5183	51.83
	1.00×10^{-4}	-549.7	419.6	116.1	-205.0	4.908	0.6215	62.15
	5.00×10^{-4}	-550.6	308.1	121.1	-185.2	3.603	0.7221	72.21
	1.00×10^{-3}	-565.7	199.5	112.7	-175.9	2.333	0.8201	82.01
DGC	1.00×10^{-5}	-530.4	649.9	112.1	-215.1	7.601	0.4138	41.38
	5.00×10^{-5}	-529.1	468.6	120.3	-184.9	5.480	0.5773	57.73
	1.00×10^{-4}	-501.7	374.8	67.3	-140.8	4.384	0.6619	66.19
	5.00×10^{-4}	-534.2	276.7	102.2	-179.1	3.236	0.7504	75.04
	1.00×10^{-3}	-571.6	175.3	110.7	-189.5	2.050	0.8419	84.19
HGC	1.00×10^{-5}	-539.3	538.8	111.3	-216.9	6.302	0.5140	51.40
	5.00×10^{-5}	-540.7	390.9	99.2	-191.6	4.572	0.6474	64.74
	1.00×10^{-4}	-543.2	290.8	100.5	-168.1	3.401	0.7377	73.77
	5.00×10^{-4}	-547.7	240.7	116.4	-172.8	2.814	0.7829	78.29
	1.00×10^{-3}	-566.4	126.9	102.0	-171.9	1.484	0.8855	88.55

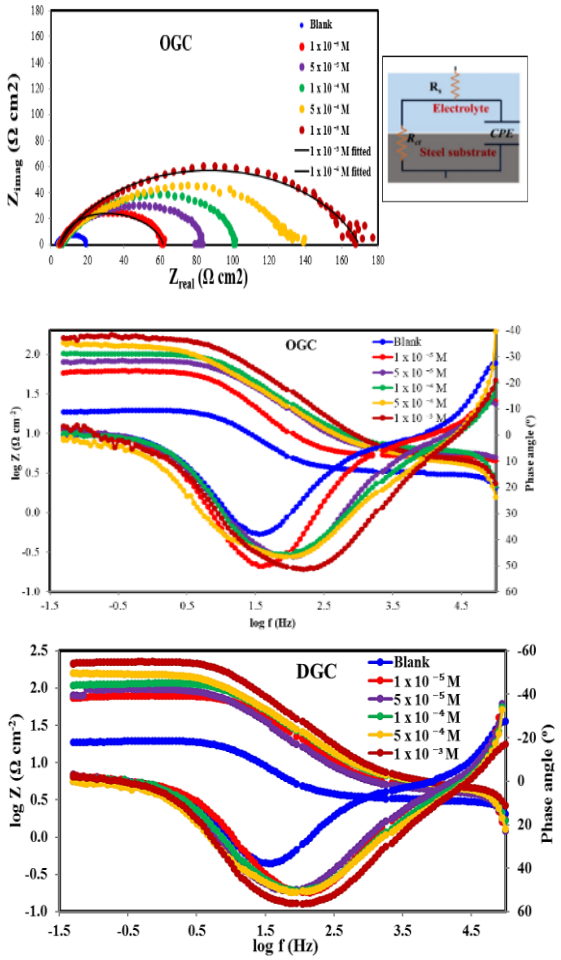

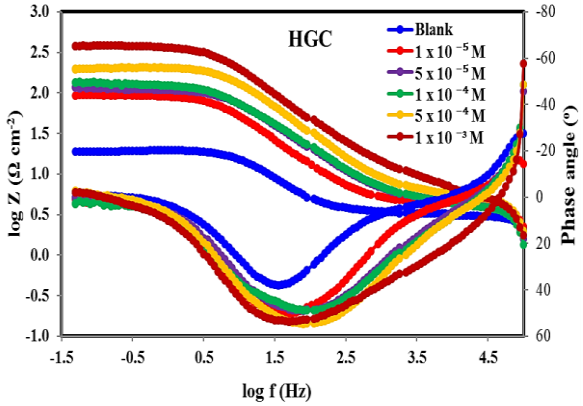

Figure 4: (A) Nyquist plots and the equivalent circuit model used to fit the EIS data; **(B)** Bode and phase angle plots of impedance spectra for the corrosion of MS in 0.5 M H_2SO_4 in the absence and presence of the synthesized cationic surfactants inhibitors (OGC, DGC, HGC) with different concentrations at 25 °C**.**

To precisely determine impedance parameters and further comprehend the influence of the heterogeneous surface, an electrical equivalent circuit model was used to fit all impedance data shown in Fig4, and the obtained results are listed in Table 5 The electrical equivalent circuit consists of the (CPE), the polarization resistance (Rct) and the solution resistance (Rs). charge transfer resistance (Rct.) **[34, 35]**.

On the other side, their inhibition efficiency (η_z) is estimated as follows:

$$\eta_z\,\% = \left(\frac{R^o_{ct} - R_{ct}}{R^o_{ct}}\right) \times 100 \quad (14)$$

where, charge transfer resistance of inhibited medium, R_{ct}, charge transfer resistance of uninhibited medium, $R^o_{ct,}$ The CPE is used to replace the real electric double-layer capacitance (Cdl) which can be replaced by CPE and the impedance of the CPE (ZCPE) can be defined according to the following equation:

$$Z_{CPE} = Y_0^{-1}(j\omega)^{-n} \quad (15)$$

where j, ω (rad.s−1), Y0 (Ω−1 sn cm−2) and n mean the imaginary unit, the angular frequency, the admittance of the CPE and the CPE exponent, respectively, in which n can be used to evaluate the surface roughness and inhomogeneity degree ($0 \le n \le 1$).

Table (4) explicates a rise in the values of R_{ct} as raising inhibitors' concentrations while corresponding values of C_{dl} decrease causing an increase in the percentage of inhibition efficacy. This may explained by a rise in adsorption of the inhibitors' molecules which function as physical barriers **[36]**. Moreover, the deficiency in values of C_{dl} is owing to either diminishing the local dielectric constant or/and expansion of the formed electrical double layer thickness via OGC, DGC and HGC inhibitors. This is perhaps ascribed to the adsorbed H_2O molecules onto MS surface displaced by the synthesized inhibitors molecules **[37]**.

R_s represent solution resistance, R_{ct} represent charge transfer resistant, Y_0, n = constant phase elements, C_{dl} = double layer capacitance, θ = surface coverage, η_z = inhibition efficiency.

Fig. 4B, Illustrates the plots of bode and phase angle of OGC, DGC and HGC inhibitors. **Table (5)** lists the increment of the inhibitors' concentrations increases the impedance parameters' values which obviously explicate formation of an impacted inhibitive layer onto steel which can protect the steel surface versus the corrosion **[38]**.

3.4. Atomic Force Microscopy

AFM proves to be an effective technique, providing insights into morphology, surface texture, and roughness. This method facilitates the acquisition of high-resolution nanoscale images and enables the examination of localized sites in electrolytes. Additionally, AFM images are used to offer a more comprehensive description of the MS surface roughness after immersion in a medium containing 0.5 mole/L of H2SO4, both in the presence and absence of Gemini inhibitors (OGC, DGC, HGC), as illustrated in Figure 5.

Table 5. EIS parameters for corrosion of MS in 0.5 M H_2SO_4 in the absence and presence of different concentrations of OGC, DGC and HGC inhibitors at 25 °C.

Inhibitor	Conc. (M)	Rs (Ru) (Ω cm2)	Rct (Rp) (Ω cm2)	Yo ($\mu\Omega^{-1}$ sn cm-2)	n	Cdl (μF cm-2)	chi squared	θ	ηz %
Blank	------	3.145	19.45	1745.00	0.8058	772.136	3.88×10^{-2}	----	-----
	1.00×10^{-5}	5.199	56.43	332.20	0.9019	215.548	1.23×10^{-2}	0.655	65.53
	5.00×10^{-5}	5.668	78.2	248.30	0.8183	103.484	4.06×10^{-3}	0.751	75.13
OGC	1.00×10^{-4}	5.873	99.65	255.10	0.7756	88.164	1.17×10^{-2}	0.805	80.48
	5.00×10^{-4}	4.211	135.1	476.10	0.7031	149.451	1.60×10^{-2}	0.856	85.60
	1.00×10^{-3}	4.611	165.3	183.20	0.7659	62.907	1.10×10^{-2}	0.882	88.23
	1.00×10^{-5}	4.401	75.13	173.80	0.849	80.342	3.59×10^{-2}	0.741	74.11
	5.00×10^{-5}	4.067	93.71	287.70	0.8108	123.808	2.35×10^{-2}	0.792	79.24
DGC	1.00×10^{-4}	4.749	114.4	206.00	0.7897	75.928	2.13×10^{-2}	0.830	83.00
	5.00×10^{-4}	4.452	158.5	268.70	0.7478	92.681	2.14×10^{-2}	0.877	87.73
	1.00×10^{-3}	4.7	229.8	129.10	0.8051	55.092	1.10×10^{-2}	0.915	91.54
	1.00×10^{-5}	4.717	84.06	30.20	0.9953	29.360	8.21×10^{-2}	0.769	76.86
	5.00×10^{-5}	4.156	113.2	324.50	0.7606	114.701	1.69×10^{-2}	0.828	82.82
HGC	1.00×10^{-4}	3.892	132.8	385.70	0.7279	127.005	1.80×10^{-2}	0.854	85.35
	5.00×10^{-4}	5.047	208.3	163.80	0.7900	66.735	1.71×10^{-2}	0.907	90.66
	1.00×10^{-3}	5.07	409.9	173.80	0.7098	59.019	2.52×10^{-2}	0.953	95.25

Clearly, the detrimental effects of corrosion on the MS surface are evident in the blank sample, showing significant damage. The absence of Gemini inhibitors is associated with a notably high average roughness (Ra) value of 97.244 nm. This elevated value suggests an aggressive attack by the corrosive environment, resulting in surface dissolution and distortion of the MS surface.

In contrast, the introduction of the synthesized Gemini inhibitors leads to a smoother surface, reduced roughness, and less corroded area compared to the blank medium, as depicted in Figure 5."The variations of average roughness are mitigated to lower values (68.856 nm, 67.087 nm and 19.278 nm) for the synthesized OGC, DGC and HGC cationic Gemini surfactants, respectively which may be because they form an effective inhibitive passive film onto MS surface that prevents MS dissolution and reduces the roughness values **[39]**

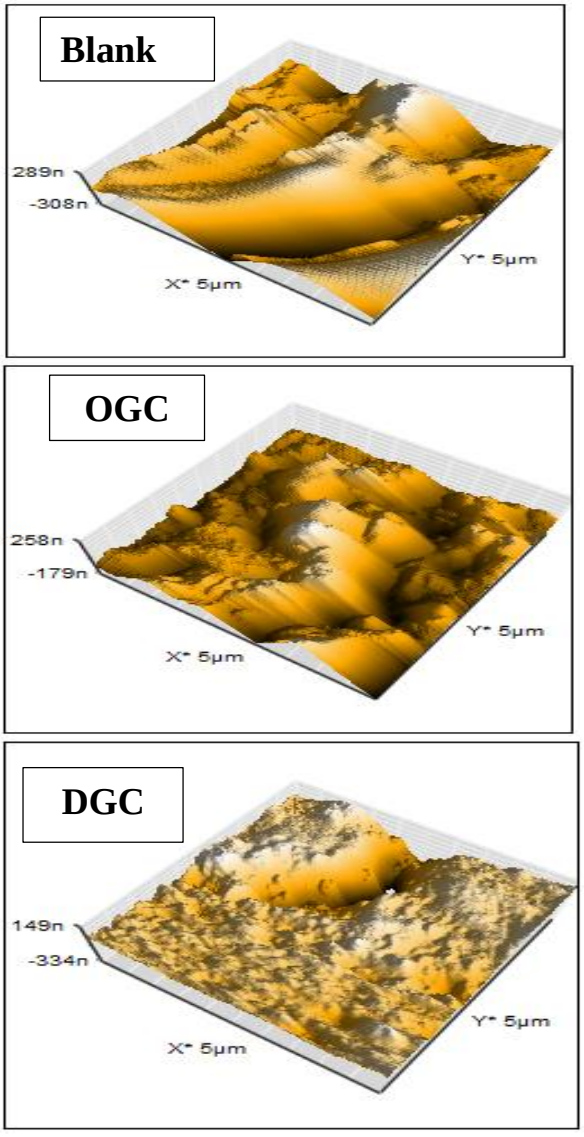

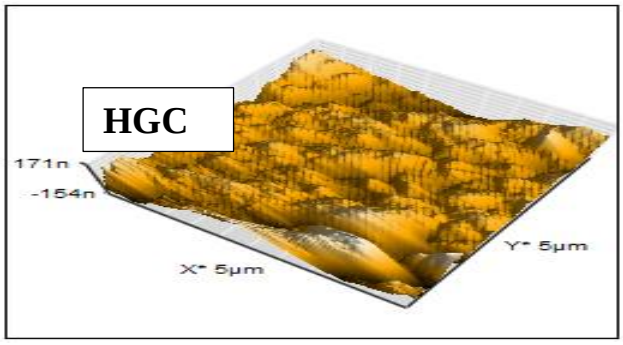

Figure 5: AFM image of the MS in 0.5 M H_2SO_4 in the absence and presence of the synthesized cationic Gemini surfactants inhibitors (OGC, DGC, HGC).

3.5. Computational approaches

3.5.1. Quantum chemical (QC) calculations

3.5.1.1. Global reactivity descriptors

QC calculations were employed to explore the electronic characteristics and molecular structure impact on the synthesized Gemini inhibitors (OGC, DGC, HGC) inhibition efficiency as well as to further support the experimental findings from electrochemical and gravemetric measurements. The optimized molecular structures for OGC, DGC and HGC inhibitors and the distribution of their highest occupied molecular orbitals, HOMOs, and lowest unoccupied molecular orbitals, LUMOs, and are shown in **Fig. 6 (a and b)**.

Fig.6 b. demonstrates that electron densities of HOMO orbitals are largely dispersed throughout the two C(O)-NH groups in the synthesized Gemini inhibitors (OGC, DGC, HGC). This implies that this site enhances the electron-donating ability among the synthesized Gemini inhibitors (OGC, DGC, HGC), which is a sign of greater interactivity. Also, it is possible for inhibitors to receive electrons from chemical species, this electron-accepting capability could be described in light of the dispersion of LUMO across the molecular structure **[40]**. The LUMO orbitals electron densities are greatly dispersed throughout the two CH_2 and CH_3 groups in the synthesized Gemini inhibitors (OGC, DGC, HGC). It reveals the synthesized Gemini inhibitors (OGC, DGC, HGC) capability to accept electrons. According to HOMO and LUMO the synthesized Gemini inhibitors (OGC, DGC, HGC) have the highest tendency to transfer and receive charges with surface of MS, consequently, they have the potential to be a powerful corrosion inhibitors **[41]**. Along with graphical representation, frontier molecular orbital (FMO) can be calculated based on their energy values, utilizing these values, electron affinity (EA) and the ionization energy (IP) can be calculated using following equations:

EA = - E_{LUMO} (16)

IP = - E_{HOMO} (17)

IP and EA values were combined to determine absolute electronegativity, χ, chemical potential, μ, and absolute hardness, η, as below:

$$x = -\mu = \frac{IP+EA}{2} \quad (18)$$

$$\eta = \frac{IP-EA}{2} \quad (19)$$

Also, the softness of the molecule (σ) can be determined using below equation:

$$\sigma = \frac{1}{\eta} \quad (20)$$

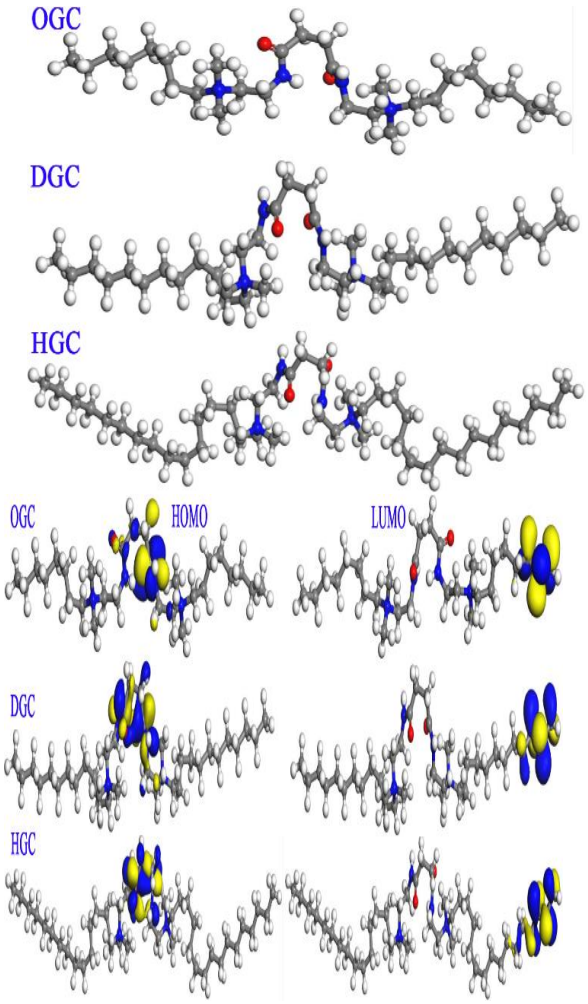

Figure 6: (a) Optimized structures of the inhibitors OGC, DGC and HGC obtained by DMol3 method, **(b)** HOMO and LUMO structures of the inhibitors OGC, DGC and HGC obtained by DMol3 method.

Table (6) show the synthesized Gemini inhibitors (OGC, DGC, HGC) quantum chemical parameters. Since HOMO is associated to electron donation, an inhibitor's high E_{HOMO} value denotes higher ability for transferring electrons to MS surface, and the higher is its inhibition efficacy. Whereas , LUMO is associated to electron acceptation, an inhibitor's lower E_{LUMO} value implies greater tendency for receiving electrons from MS surface and the higher is its inhibition efficacy **[42, 43]**. By inspecting the findings in **Table (6)**, E_{HOMO} values for the synthesized Gemini inhibitors (OGC, DGC, HGC) in gas phases by DMol3 method revealed that HGC inhibitor that poses the greatest inhibition efficiency, has the greatest value of E_{HOMO}. The increasing E_{HOMO} values aligns well with the order found in the experimental data HGC > DGC > OGC. Whereas it appears that the E_{LUMO} values do not stick to the same sequence. This suggests that, however LUMO is a crucial factor, it does not incisive in assessing the synthesized Gemini inhibitors (OGC, DGC, HGC) corrosion inhibition efficiency. Moreover, HOMO-LUMO gap (ΔE) is a remarkable factor in determining the stability of the synthesized inhibitors and their reactivity **[39]**. Large values ΔE indicates low reactivity and high electronic stability. Whereas, low ΔE values implies greater reactivity, since it is easier for electrons to become excited and shift from HOMO to LUMO, and as a result, the adsorption ability on MS surface increases consequently the inhibition efficiency increases **[44, 45]**. From data in **Table (6)**, HGC inhibitor poses the least value of ΔE with value of 2.1830 eV, which indicates that HGC inhibitor poses the highest reactivity and so the highest MS corrosion inhibition efficiency. Whereas OGC inhibitor poses the highest value of ΔE with value of 3.2988 eV, which indicates that OGC inhibitor poses the least reactivity and so the least MS corrosion inhibition efficiency among the synthesized Gemini inhibitors (OGC, DGC, HGC).

The interaction between OGC, DGC and HGC inhibitors and the surface of MS can be discussed using hard soft acid base, HSAB, conditions and frontier controlled interaction principles. The theory states that, hard acids like paring with hard bases while soft acids like paring with soft bases. While HOMO-LUMO gap for soft molecules is small, it is much larger for hard molecules [43]. Furthermore, the best inhibitors for metals are soft bases inhibitors because metal atoms are considered soft acids. As a result, increasing softness will increase the inhibition efficiency. According to data in **Table (6)**, HGC inhibitor poses the highest σ with 0.9162 eV^{-1} value and the lowest hardness with 1.0915 eV value which indicates that HGC inhibitor poses the greatest reactivity and, hence, the greatest efficiency of inhibition.. Additionally, OGC inhibitor has the lowest σ with 0.6063 eV^{-1} value and the highest hardness with 1.6494 eV value which indicates that OGC inhibitor poses the least reactivity and, hence, the least efficiency of inhibition.

Table 6. The calculated quantum chemical parameters in eV for the inhibitors at DMol3 in gas phase and in aqueous phase

	Molecule	E_{HOMO}	E_{LUMO}	ΔE	$\Delta E_{back\ donation}$	T.E.	ε	σ	ω	χ	ΔN	ΔN_{max}	η	IE
		(eV)	(eV)	(eV)	(eV)	(eV)	(eV^{-1})	(eV^{-1})	(eV)	(e)	(e)	(e)	(eV)	(%)
gas	OGC	-10.17	-6.87	3.29	-0.41	-39667.44	22.01	0.60	0.0454	8.52	-1.12	5.16	1.64	88.2
gas	DGC	-9.32	-6.36	2.95	-0.36	-48137.52	20.81	0.67	0.0480	7.84	-1.02	5.30	1.47	91.5
gas	HGC	-8.93	-6.75	2.18	-0.27	-56607.40	28.18	0.91	0.0355	7.84	-1.38	7.18	1.09	95.2
aqueous	OGC	-6.02	-1.62	4.39	-0.54	-39672.99	3.32	0.45	0.3006	3.82	0.22	1.73	2.19	88.2
aqueous	DGC	-6.13	-1.43	4.70	-0.58	-48142.79	3.04	0.42	0.3287	3.78	0.22	1.60	2.35	91.5
aqueous	HGC	-6.27	-1.61	4.66	-0.58	-56613.01	3.34	0.42	0.2992	3.94	0.18	1.69	2.33	95.2

The nucleophilicity index, *ε*, and its reverse index, the electrophilicity index, *ω*, were estimated using below equations **[46, 47]**:

$$\omega = \frac{\mu^2}{2\,\eta} \qquad (21)$$

$$\varepsilon = \frac{1}{\omega} \qquad (22)$$

Electrophilicity and chemical potential are two ways to assess a molecule's ability to accept electrons. On the other side, the electron sharing ability is related to nucleophilicity. The molecule that has the lowest *ω* values and highest *ε* values will exhibits high inhibition efficiency **[48]**. Findings in **Table (6)**, showed that HGC inhibitor molecules poses the lowest *ω* values with values of 0.0355 and 0.2992 eV in both gas and aqueous phases, respectively. Furthermore, HGC inhibitor molecules poses the greatest *ε* values with 28.1844 and 3.3420 eV^{-1} values in gas phase and aqueous phase, respectively. So, HGC inhibitor poses the greatest MS corrosion inhibition efficiency **[48, 49]**.

Additionally, in corrosion investigations, the number of electrons transferred from OGC, DGC and HGC inhibitors to MS surface, ΔN, and the maximum number of transferred electrons, ΔN_{max}, can be evaluated using the below formulas **[50, 51]**.

$$\Delta N = \frac{\chi_{Fe} - \chi_{inh}}{2(\eta_{Fe} + \eta_{inh})} \qquad (23)$$

$$\Delta N_{max} = \frac{\chi}{2\,\eta} \qquad (24)$$

where, χ_{Fe}, χ_{inh}, η_{Fe}, η_{inh}, η and χ are Fe electronegativity, inhibitor electronegativity, Fe metal hardness and inhibitor hardness, absolute hardness and absolute electronegativity, respectively. ΔN provides valuable data about the inhibitor molecules capability to receive/or share electrons from/to the surface of the metal. If ΔN > 0, the inhibitor molecule can denote its electron to the metal, the opposite is true if ΔN < 0 **[52, 53]**. From data in **Table (6)**, the positive ΔN values for OGC, DGC and HGC inhibitors in aqueous phases indicates the inhibitors molecules ability to share electrons with MS surface **[46]**. In addition, the data demonstrated that ΔN_{max} was higher than before via the identical ranking achieved from the experiment data, which show that HGC poses the greatest efficiency of inhibition while OGC poses the least efficiency of inhibition. The binding of the synthesized Gemini inhibitors (OGC, DGC, HGC) molecules to MS surface may be controlled by the electron back donation from MS to inhibitors molecules referring to the charge transfer model proposed by Gomez et al. **[54]** which linked the energy of back donation, $\Delta E_{back\text{-}donation}$, by the hardness of the inhibitor molecules, η, assuming both the electron donation and electron back donation processes occur according to the formula;

$$\Delta E_{back-donation} = -\frac{\eta}{4} \qquad (25)$$

The values of $\Delta E_{back\text{-}donation}$ were negative implies the favourability of the follow of electrons from MS to inhibitors molecules. A powerful adsorption and high inhibition efficiency may result from a rise in the $\Delta E_{back\text{-}donation}$. The $\Delta E_{back\text{-}donation}$ values for the synthesized Gemini inhibitors (OGC, DGC, HGC) in gas phases by DMol3 method are -0.4123, -0.3695 and -0.2729 for OGC, DGC, HGC, respectively.

3.5.1.2. Local Reactivity: Fukui Functions.

One of the best theoretical techniques for determining chemical molecule's reactivity and selectivity is the use of Fukui function indices **[55]**. Fukui functions enable us to identify the inhibitor atomic sites where the electron donation or acceptance is greatest, indicating the likelihood that this site will be attacked by an electrophile or a nucleophile. The nucleophilic sites, f_k^+, electrophilic sites, f_k^-, and the dual descriptor, Δf_k, can be determined by the below formulas **[56, 57]**:

$$f_k^+ = q_k(N+1) - q_k(N) \qquad (26)$$

$$f_k^- = q_k(N) - q_k(N-1) \qquad (27)$$

$$\Delta f_k = f_k^+ - f_k^- \qquad (28)$$

where q_k represents the atomic charge in its anionic $(N+1)$, neutral (N), or cationic $(N-1)$ state. The advantage of employing dual descriptor, Δf_k, is the ability to precisely identify both acceptor sites (If $\Delta f_k > 0$) and donor sites sites (If $\Delta f_k < 0$). The obtained results of the fukui indices for electrophilic centers and nucleophilic centers for the synthesized Gemini inhibitors (OGC, DGC, HGC) are cited in **Table (7)**. From findings, the acceptor sites extremely vulnerable to nucleophilic attack, that have a $\Delta f_k > 0$, are OGC: O(20) with a value of 0.155, DGC: C(19) with a value of 0.108 and HGC: O(23) with a value of 0.107. whereas, the donor sites extremely vulnerable to electrophilic attack, which have a $\Delta f < 0$, are OGC: C(16) with a value of -0.034, DGC: C(17) with a value of -0.074 and HGC: C(17) with a value of -0.029.

3.5.2. Mont carlo (MC) simulations

The adsorption mechanism of OGC, DGC, and HGC inhibitors on MS surface has been clarified using MC simulations. **Fig. 7** displays the geometrical structures for the most appropriate configuration for the adsorption of OGC, DGC, and HGC inhibitors molecules on MS Surface. The interactive force of inhibitor molecules is significantly depending on two main aspects; the molecules orientation and the adsorption active sites, such as heteroatoms. It is anticipated that molecules that incorporate these two factors will have a high corrosion inhibition efficiency. Examining our findings reveals that inhibitor molecules were adsorbed with a parallel orientation on MS surface.

Undoubtedly, the parallel orientation will increase the blocked surface area and interactions between the active sites of molecules and MS atoms, resulting in a higher inhibition efficiency. Another technique used to understand the interactivity of molecules involves evaluating the interactions and binding energy once the adsorption system reaches a steady state. Inhibitor molecules interaction and binding energies are cited in **Table (8).** From findings in **Table (8)**, the synthesized Gemini inhibitors (OGC, DGC, HGC) adsorption energy values were negative, indicating spontaneous adsorption process. The binding energy values for the synthesized Gemini inhibitors (OGC, DGC, HGC) in gas phases by Monte Carlo simulation are 354.632, 432.604 and 489.356 kcal/mol for OGC, DGC, HGC, respectively.

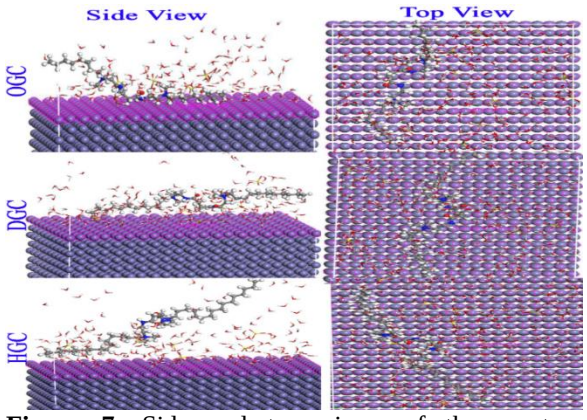

Figure 7: Side and top views of the most appropriate configuration for adsorption of (OGC, DGC and HGC) molecules on MS Surface obtained by MC simulations in the aqueous solution.

Furthermore, the values of binding energy for the synthesized Gemini inhibitors (OGC, DGC, HGC) in aqueous phases by Monte Carlo simulation are 357.131, 413.839 and 457.271 kcal/mol for OGC, DGC, HGC, respectively. The arrangement of binding energy supports the arrangement of the experimental results. The inhibitor molecule's high binding energy reflects both its strong interaction with MS surface and higher adsorption to MS surface **[58, 59]**.

3.6. Silver Nano structures confirmation

In current study, the Ag NPs were prepared using the photo-reduction method**[18, 60]** For controlling their morphological structure, sun rays had utilized as a strong reducing agent in existence of these synthetic amphiphiles as a capping agent. Then, the radiation of sunlight will release H_2, H_2O_2, $H^{\bullet}$, $OH^{\bullet}$ by water radiolysis while the released electron acts as moieties promoting $AgNO_3$ precursor reduction into Ag NPs. Amphiphiles plays a significant role in reduction process of silver to silver Nano particles lead to diminished the process time. both free radical of $H^{\bullet}$ and free radical of $OH^{\bullet}$ should be consumed and their concentrations should be diminished in presence of these surfactants, causing further sunlight radiolysis and thus continually producing active species**[61]**. The kinetics of reduction process had raised into few minutes as it's concentration of liberated H_2O_2 and solvated electrons in the presence of these surfactants increase. Their hydrophobic tail was critical in controlling the Ag NPs morphological structure as evident in Figures 8a,8b and 8c. The three surfactants unite forming spherical AgNPs, whereas the particle distribution varies as depicted in TEM Figures 8a,8b and 8c.

Table 7. Condensed Fukui functions and dual descriptor of OGC, DGC and HGC obtained by DMol^3 method.

Atom	**OGC**			Atom	**DGC**			Atom	**HGC**		
	f^+	f^-	Δf		f^+	f^-	Δf		f^+	f^-	Δf
C (1)	-0.008	0	-0.008	C (1)	-0.004	-0.008	0.004	C (1)	-0.001	0	-0.001
C (2)	-0.008	-0.002	-0.006	C (2)	-0.008	0.003	-0.011	C (2)	-0.003	0	-0.003
C (3)	-0.002	-0.002	0	C (3)	-0.009	0	-0.009	C (3)	-0.003	0.001	-0.004
C (4)	-0.002	-0.005	0.003	C (4)	-0.005	0.003	-0.008	C (4)	0	-0.001	0.001
C (5)	-0.004	-0.011	0.007	C (5)	-0.012	0.006	-0.018	C (5)	-0.002	-0.001	-0.001
C (6)	-0.002	-0.024	0.022	C (6)	0.011	-0.016	0.027	C (6)	-0.002	-0.001	-0.001
C (7)	-0.002	-0.032	0.03	C (7)	0	-0.007	0.007	C (7)	-0.001	-0.002	0.001
C (8)	-0.001	-0.016	0.015	C (8)	0.007	-0.02	0.027	C (8)	-0.004	-0.001	-0.003
N (9)	-0.003	0	-0.003	C (9)	0.001	-0.022	0.023	C (9)	-0.001	-0.003	0.002
C (10)	-0.009	-0.001	-0.008	C (10)	0.006	-0.039	0.045	C (10)	-0.001	-0.006	0.005
C (11)	-0.018	-0.001	-0.017	C (11)	0.004	-0.042	0.046	C (11)	-0.001	-0.007	0.006
C (12)	-0.013	-0.001	-0.012	C (12)	0.006	-0.026	0.032	C (12)	-0.001	-0.012	0.011
C (13)	-0.033	-0.001	-0.032	N (13)	-0.006	0.005	-0.011	N (13)	-0.004	0	-0.004
N (14)	0.07	0	0.07	C (14)	-0.012	0.005	-0.017	C (14)	0	0	0
C (15)	0.139	-0.002	0.141	C (15)	0	-0.009	0.009	C (15)	-0.009	0	-0.009
C (16)	-0.034	0	-0.034	C (16)	-0.002	-0.008	0.006	C (16)	-0.001	0	-0.001
C (17)	-0.013	0	-0.013	C (17)	-0.048	0.026	-0.074	C (17)	-0.029	0	-0.029
C (18)	0.001	0.002	-0.001	N (18)	0.053	-0.005	0.058	N (18)	0.022	-0.001	0.023
O (19)	0.069	0.013	0.056	C (19)	0.09	-0.018	0.108	C (19)	0.05	-0.001	0.051
O (20)	0.155	0	0.155	C (20)	-0.01	-0.008	-0.002	C (20)	-0.025	0	-0.025
N (21)	-0.028	0.004	-0.032	C (21)	0.014	-0.018	0.032	C (21)	-0.028	0	-0.028
C (22)	-0.005	-0.003	-0.002	C (22)	0.039	-0.018	0.057	C (22)	0.072	0.001	0.071
C (23)	0	-0.003	0.003	O (23)	0.049	0.02	0.029	O (23)	0.108	0.001	0.107
N (24)	-0.002	-0.001	-0.001	O (24)	0.104	0.01	0.094	O (24)	0.103	0.002	0.101
C (25)	-0.006	-0.001	-0.005	N (25)	0.032	0.001	0.031	N (25)	0.034	0.001	0.033
C (26)	-0.003	-0.001	-0.002	C (26)	-0.005	-0.01	0.005	C (26)	-0.02	0	-0.02
C (27)	-0.005	0	-0.005	C (27)	-0.021	0.02	-0.041	C (27)	-0.006	0	-0.006
C (28)	-0.004	-0.003	-0.001	N (28)	0	-0.002	0.002	N (28)	-0.002	0	-0.002
C (29)	-0.003	-0.002	-0.001	C (29)	-0.001	-0.003	0.002	C (29)	-0.008	0	-0.008
C (30)	-0.002	-0.005	0.003	C (30)	0.014	-0.022	0.036	C (30)	-0.009	0	-0.009
C (31)	-0.003	-0.012	0.009	C (31)	-0.006	-0.004	-0.002	C (31)	-0.013	0	-0.013
C (32)	-0.002	-0.025	0.023	C (32)	0.006	-0.008	0.014	C (32)	0	-0.001	0.001
C (33)	-0.002	-0.035	0.033	C (33)	0.018	-0.022	0.04	C (33)	-0.004	0	-0.004
C (34)	-0.001	-0.018	0.017	C (34)	-0.017	0.011	-0.028	C (34)	-0.006	0.001	-0.007
				C (35)	0.001	-0.005	0.006	C (35)	-0.001	0	-0.001
				C (36)	-0.007	0.003	-0.01	C (36)	-0.006	0	-0.006
				C (37)	0.003	-0.008	0.011	C (37)	0	-0.002	0.002
				C (38)	-0.002	-0.006	0.004	C (38)	-0.002	-0.001	-0.001
				C (39)	-0.001	-0.012	0.011	C (39)	-0.001	-0.004	0.003
				C (40)	0	-0.022	0.022	C (40)	-0.001	-0.005	0.004
				C (41)	-0.003	-0.024	0.021	C (41)	-0.001	-0.006	0.005
				C (42)	0.005	-0.018	0.023	C (42)	-0.001	-0.01	0.009
								C (43)	-0.001	-0.016	0.015
								C (44)	-0.001	-0.024	0.023
								C (45)	-0.001	-0.025	0.024
								C (46)	-0.001	-0.014	0.013
								C (47)	-0.001	-0.014	0.013
								C (48)	-0.001	-0.02	0.019
								C (49)	-0.001	-0.02	0.019
								C (50)	-0.001	-0.012	0.011

Table 8. The outputs and descriptors calculated by the Monte Carlo simulation for adsorption of OGC, DGC and HGC on MS (in kcal/ mol).

phase	inhibitor	Total energy ($kcalmol^{-1}$)	Adsorption energy ($kcalmol^{-1}$)	Rigid adsorption energy ($kcalmol^{-1}$)	Deformation energy ($kcalmol^{-1}$)	($dE_{ads/dNi}$) ($kcalmol^{-1}$)	Binding energy ($kcalmol^{-1}$)	IE* (%)
Gas phase	OGC	-230.06	-354.63	-314.29	-40.33	-354.63	354.63	88.23
	DGC	-309.46	-432.60	-383.48	-49.12	-432.60	432.60	91.54
	HGC	-391.14	-489.35	-449.66	-39.68	-489.35	489.35	95.25
Aqueous phase	OGC	-8704.93	-9036.39	-9029.41	-6.97	-357.13	357.13	88.23
	DGC	-8705.16	-9047.38	-9046.13	-0.87	-413.83	413.83	91.54
	HGC	-8719.10	-9047.76	-9046.89	-1.25	-457.27	457.27	95.25

On the other hand, raising the surfactant hydrophobic tail results in more regular Ag NPs with excellent stable colloid and this is credited to higher affinity of amphiphile's adsorption with a longer lipophilic carbon chain contrasted to a shorter carbon chain. The HGC surfactant with longer chain length supplied more adjusted, distributed, and smaller size of Ag NPs particles (Figure. 8c), whereas OGC surfactant with less lipophilic chain length (8 carbon atoms) provided irregular shape and semi aggregated spherical Ag NPs (Figure. 8a)

Besides, the particle size of the fabricated Ag NPs (Figures. 8a–c) had estimated by the number of carbon atoms in hydrophobic tail. Hence, the particle sizes of the synthesized OGC/Ag NPs, DGC/Ag NPs, and HGC/Ag NPs hybrid systems are 91.28, 78.82, and 58.77 nm, progressively (Figures 8d,8e,8f).

Undoubtedly, these findings reinforce the potential of amphiphile's lipophilic chain length in regulating the size of particle size which for in-situ synthesized

Ag NPs decreases as the surfactant tail length increases, resulting in more uniform and stable particles. On the other hand, the measured zeta potentials reveal the Ag NPs stability strongly depend on the lipophilic chain. The zeta potentials of the OGC/AgNPs, DGC/AgNPs, and HGC/AgNPs mixed systems was 44.0 ± 9.34, 70.8 ± 6.46, and 87.6 ± 15.5 mV, respectively, which increased as surfactant tail length raises.**[18]**

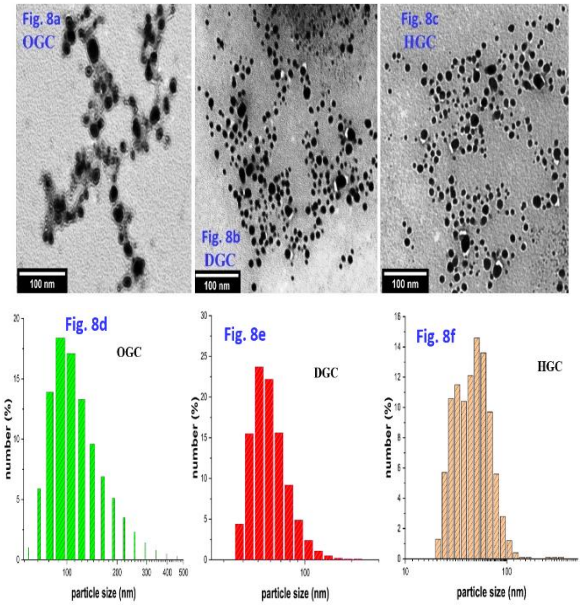

Figures. 8a,8b,8c. TEM images of prepared OGC,DGC and HGC capped Ag/Nano particles. Figurers 8d,8e,8f Size distribution of prepared OGC,DGC and HGC capped Ag/Nano particles.

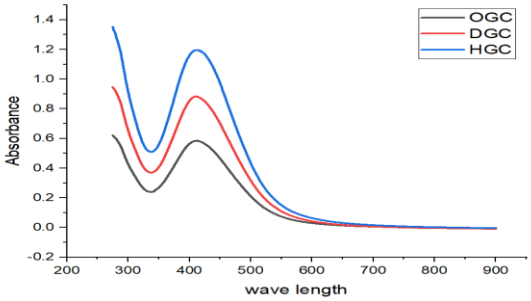

Figure 9. UV spectra of prepared OGC,DGC and HGC capped Ag/Nano particles.

4. Conclusions

- The three surfactants under investigation are very effective as a corrosion inhibitor for MS in acid media.
- Increased inhibitor concentrations and temperatures enhance inhibition efficiency against corrosion, reaching 95.25% with 1x10-3 M HGC via EIS measurements, and they act as mixed-type corrosion inhibitors.
- Consistent findings across multiple analytical techniques validate the accuracy and reliability of the study's outcomes.
- Modified Langmuir's model (Villamil's isotherm) confirms inhibitor molecule adsorption on metal surfaces.
- AFM analysis affirms the suitability of cationic Gemini surfactants as effective anti-corrosive agents.
- Computational data supports experimental results, shedding light on molecular-level interactions and corrosion inhibition mechanisms.
- Gemini surfactants also exhibit potential as capping agents, stabilizing silver nanoparticles, as evidenced by measured zeta potentials.
- The study unveils the dual functionality of these surfactants, with broader applications in anti-corrosion coatings and nanotechnology.
- Future exploration could reveal novel dimensions for these compounds, expanding their role in materials science and corrosion prevention.

5. Conflict of interest

There are no conflicts to declare.

6. Acknowledgments

The authors thankful to Egyptian Petroleum Research Institute.

7. References

[1]L.O. Olasunkanmi, I.B. Obot, M.M. Kabanda, E.E. Ebenso, Some Quinoxalin-6-yl Derivatives as Corrosion Inhibitors for Mild Steel in Hydrochloric Acid: Experimental and Theoretical Studies, Journal of Physical Chemistry C, 119 (2015) 16004-16019.

[2]J. Cui, Y.G. Yang, X.Q. Li, W.J. Yuan, Y.S. Pei, Toward a Slow-Release Borate Inhibitor To Control Mild Steel Corrosion in Simulated Recirculating Water, Acs Applied Materials & Interfaces, 10 (2018) 4183-4197.

[3]Y. El Aoufir, R. Aslam, F. Lazrak, R. Marzouki, S. Kaya, S. Skal, A. Ghanimi, I.H. Ali, A. Guenbour, H. Lgaz, I.M. Chung, The effect of the alkyl chain length on corrosion inhibition performances of 1,2,4-triazole-based compounds for mild steel in 1.0 M HCl: Insights from experimental and theoretical studies, Journal of Molecular Liquids, 303 (2020).

[4]A. Dehghani, G. Bahlakeh, B. Ramezanzadeh, M. Ramezanzadeh, A combined experimental and theoretical study of green corrosion inhibition of mild steel in HCl solution by aqueous Citrullus lanatus fruit (CLF) extract, Journal of Molecular Liquids, 279 (2019) 603-624.

[5]M.K. Awad, M.S. Metwally, S.A. Soliman, A.A. El-Zomrawy, M.A. Bedair, Experimental and quantum chemical studies of the effect of poly ethylene glycol as corrosion inhibitors of aluminum surface, Journal of Industrial and Engineering Chemistry, 20 (2014) 796-808.

[6]E. Alibakhshi, M. Ramezanzadeh, S.A. Haddadi, G. Bahlakeh, B. Ramezanzadeh, M. Mandavian, Persian Liquorice extract as a highly efficient sustainable corrosion inhibitor for mild steel in sodium chloride solution, Journal of Cleaner Production, 210 (2019) 660-672.

[7]P. Singh, E.E. Ebenso, L.O. Olasunkanmi, I.B. Obot, M.A. Quraishi, Electrochemical, Theoretical, and Surface Morphological Studies of Corrosion Inhibition Effect of Green Naphthyridine Derivatives on Mild Steel in Hydrochloric Acid, Journal of Physical Chemistry C, 120 (2016) 3408-3419.

[8]Y.M. Panchenko, A.I. Marshakov, Long-term prediction of metal corrosion losses in atmosphere using a power-linear function, Corrosion Science, 109 (2016) 217-229.

[9]S. Pareek, D. Jain, S. Hussain, A. Biswas, R. Shrivastava, S.K. Parida, H.K. Kisan, H. Lgaz, I.M. Chung, D. Behera, A new insight into corrosion inhibition mechanism of copper in aerated 3.5 wt.% NaCl solution by eco-friendly Imidazopyrimidine Dye: experimental and theoretical approach, Chemical Engineering Journal, 358 (2019) 725-742.

[10]X.H. Luo, X.Y. Pan, S. Yuan, S. Du, C.X. Zhang, Y.L. Liu, Corrosion inhibition of mild steel in simulated seawater solution by a green eco-friendly mixture of glucomannan (GL) and bisquaternary ammonium salt (BQAS), Corrosion Science, 125 (2017) 139-151.

[11]M.A. Deyab, Hydrogen generation during the corrosion of carbon steel in crotonic acid and using some organic surfactants to control hydrogen evolution, International Journal of Hydrogen Energy, 38 (2013) 13511-13519.

[12]M. Mahdavian, A.R. Tehrani-Bagha, K. Holmberg, Comparison of a Cationic Gemini Surfactant and the Corresponding Monomeric Surfactant for Corrosion Protection of Mild Steel in Hydrochloric Acid, Journal of Surfactants and Detergents, 14 (2011) 605-613.

[13]O. Kaczerewska, R. Leiva-Garcia, R. Akid, B. Brycki, I. Kowalczyk, T. Pospieszny, Effectiveness of O-bridged cationic gemini surfactants as corrosion inhibitors for stainless steel in 3 M HCl: Experimental and theoretical

studies, Journal of Molecular Liquids, 249 (2018) 1113-1124.

[14]A.A. Farag, H.E. Abdallah, E.A. Badr, E.A. Mohamed, A.I. Ali, A.Y. El-Etre, The inhibition performance of morpholinium derivatives on corrosion behavior of carbon steel in the acidized formation water: Theoretical, experimental and biocidal evaluations, Journal of Molecular Liquids, 341 (2021).

[15]A.K. Al-Edan, W.N. Roslam Wan Isahak, Z.A. Che Ramli, W.K. Al-Azzawi, A.A.H. Kadhum, H.S. Jabbar, A. Al-Amiery, Palmitic acid-based amide as a corrosion inhibitor for mild steel in 1M HCl, Heliyon, 9 (2023) e14657.

[16]M. Guo, Y. Zhang, F. Du, Y. Wu, Q. Zhang, C. Jiang, Silver nanoparticles/polydopamine coated polyvinyl alcohol sponge as an effective and recyclable catalyst for reduction of 4-nitrophenol, Materials Chemistry and Physics, 225 (2019) 42-49.

[17]E.A. Badr, S.H. Shafek, H.H.H. Hefni, A.M. Elsharif, A.A. Alanezi, S.M. Shaban, D.-H. Kim, Synthesis of Schiff base-based cationic Gemini surfactants and evaluation of their effect on in-situ AgNPs preparation: Structure, catalytic, and biological activity study, Journal of Molecular Liquids, 326 (2021) 115342.

[18]S.M. Shaban, E.H.I. Ismael, A.M. Elsharif, A.H. Elged, N.M. El Basiony, Preparation gemini non-ionic surfactants-based polyethylene oxide with variable hydrophobic tails for controlling the catalytic and antimicrobial activity of AgNPs, Journal of Molecular Liquids, 367 (2022) 120416.

[19]M.G. Gab-Allah, A.H. El-Ged, E.A. Badr, M.A. Bedair, S.A. Soliman, M.F. Bakr, Three novel Gemini amide amphiphilics synthesis, characterization, thermodynamics, surface properties and biological activity, Egyptian Journal of Petroleum, 32 (2023) 27-33.

[20]A.H. Elged, S.M. Shaban, M. Eluskkary, I. Aiad, E. Soliman, A.M. Elsharif, D.-H.J.J.o.I. Kim, E. Chemistry, Impact of hydrophobic tails of new phospho-zwitterionic surfactants on the structure, catalytic, and biological activities of AgNPs, 94 (2021) 435-447.

[21]S.M. Shaban, E.H. Hamed, A.M. Elsharif, A.H. Elged, N.J.J.o.M.L. El Basiony, Preparation gemini non-ionic surfactants-based polyethylene oxide with variable hydrophobic tails for controlling the catalytic and antimicrobial activity of AgNPs, 367 (2022.120416 (

[22]A.M. Hassan, B.H. Heakal, A. Younis, M.A. Bedair, Z.I. Elbialy, M.M. Abdelsalam, Synthesis of Some Triazole Schiff Base Derivatives and Their Metal Complexes under Microwave Irradiation and Evaluation of Their Corrosion Inhibition and Biological Activity, Egyptian Journal of Chemistry, 62 (2019) 1603-1624.

[23]D.Q. Xu, X.Y. Ni, C.Y. Zhang, J. Mao, C.C. Song, Synthesis and properties of biodegradable cationic gemini surfactants with diester and flexible spacers, Journal of Molecular Liquids , .548-542 (2017) 240

[24]T. Zhou, J. Yuan, Z.Q. Zhang, X. Xin, G.Y. Xu, The comparison of imidazolium Gemini surfactant C-14-4-C(14)im Br-2 and its corresponding monomer as corrosion inhibitors for A3 carbon steel in hydrochloric acid solutions: Experimental and quantum chemical studies, Colloids and Surfaces a-Physicochemical and Engineering Aspects, 575 (2019) 57-65.

[25]M.A. Bedair, S.A. Soliman, M.F. Bakr, E.S. Gad, H. Lgaz, I.M. Chung, M. Salama, F.Z. Alqahtany, Benzidine-based Schiff base compounds for employing as corrosion inhibitors for carbon steel in 1.0 M HCl aqueous media by chemical, electrochemical and computational methods, Journal of Molecular Liquids, 317 (2020).

[26]X.M. Wang, H.Y. Yang, F.H. Wang, A cationic gemini-surfactant as effective inhibitor for mild steel in HCl solutions, Corrosion Science, 52 (2010) 1268-1276.

[27]M.A. Mostafa, A.M. Ashmawy, M. Reheim, M.A. Bedair, A.M. Abuelela, Molecular structure aspects and molecular reactivity of some triazole derivatives for corrosion inhibition of aluminum in 1 M HCl solution, Journal of Molecular Structure, 1236 (2021).

[28]M.A. Bedair, A.M. Abuelela, W.M. Zoghaib, T.A. Mohamed, Molecular structure, tautomer's, reactivity and inhibition studies on 6-Methyl-2-thiouracil for mild steel corrosion in aqueous HCl (1.00 M): Experimental and Theoretical Studies, Journal of Molecular Structure, 1244 (2021).

[29]S.A. Soliman, M.S. Metwally, S.R. Selim, M.A. Bedair, M.A. Abbas, Corrosion inhibition and adsorption behavior of new Schiff base surfactant on steel in acidic environment: Experimental and theoretical studies, Journal of Industrial and Engineering Chemistry, 20 (2014) 4311-4320.

[30]N.A. Negm, S.A. Ahmed, E.A. Badr, M.A. Ghani, M.A. El-Raouf, Synthesis and Evaluation of Nonionic Surfactants Derived from Tannic Acid as Corrosion Inhibitors for Carbon Steel in Acidic Medium, 18 (2015) 989-1001.

[31]E.A. Ghiaty, D.E. Mohamed, E.A. Badr, E.A.M. Gad, E.A. Soliman, I.A. Aiad, Experimental and Computational Study of Ecofriendly Synthesize d Imine Cationic Surfactants as Corrosion Inhibitors for Carbon Steel in 1 M HCl, 57 (2020) 45-56.

[32]S.S. Alarfaji, I.H. Ali, M.Z. Bani-Fwaz, M.A. Bedair, Synthesis and Assessment of Two Malonyl Dihydrazide Derivatives as Corrosion Inhibitors for Carbon Steel in Acidic Media: Experimental and Theoretical Studies, Molecules, 26 (2021).

[33]M.M. Abdelsalam, M.A. Bedair, A.M. Hassan, B.H. Heakal, A. Younis, Z.I. Elbialy, M.A. Badawy, H.E.D. Fawzy, S.A. Fareed, Green synthesis, electrochemical, and DFT studies on the corrosion inhibition of steel by some novel triazole Schiff base derivatives in hydrochloric acid solution, Arabian Journal of Chemistry, 15 (2022).

[34]R. Haldhar, S.C. Kim, D. Prasad, M.A. Bedair, I. Bahadur, S. Kaya, O. Dagdag, L. Guo, Papaver somniferum as an efficient corrosion inhibitor for iron alloy in acidic condition: DFT, MC simulation, LCMS and electrochemical studies, Journal of Molecular Structure, 1242 (2021).

[35]S.M. Tawfik, A.S. Kobisy, E.A. Badr, A.H. Elged, Y.I. Lee, Surface-active nonionic conjugated zirconium metal–organic frameworks and their applications; Broad spectrum anti-microbial, anti-SRB biofilm, anti-microbial corrosion, Environmental Technology and Innovation, 29 (2023).

[36]A.M.A. Nour, N.A. Negm, G.H. Sayed, S.M. Tawfik, E.A. Badr, Quantum Chemical and Electrochemical Evaluation of Alkyl Phosphine Oxide in Corrosion Inhibition of Carbon Steel in Formation Water, Zeitschrift Fur Physikalische Chemie-International Journal of Research in Physical Chemistry & Chemical Physics, 233 (2019) 1761-1785.

[37]M.A. Abbas, M.A. Bedair, O.E. El-Azabawy, E.S. Gad, Anticorrosion Effect of Ethoxylate Sulfanilamide Compounds on Carbon Steel in 1 M Hydrochloric Acid: Electrochemical and Theoretical Studies, Acs Omega, 6 (2021) 15089-15102.

[38]M.A. Bedair, S.A. Soliman, M.A. Hegazy, I.B. Obot, A.S. Ahmed, Empirical and theoretical investigations on the corrosion inhibition characteristics of mild steel by three new Schiff base derivatives, Journal of Adhesion Science and Technology, 33 (2019) 1139-1168.

[39]M.A. Bedair, A.S. Fouda, M.A. Ismail, A. Mostafa, Inhibitive effect of bithiophene carbonitrile derivatives on carbon steel corrosion in 1M HCl solution: experimental and theoretical approaches, Ionics, 25 (201.2933-2913 (9

[40]H. Lgaz, R. Salghi, K.S. Bhat, A. Chaouiki, Shubhalaxmi, S. Jodeh, Correlated experimental and theoretical study on inhibition behavior of novel quinoline derivatives for the corrosion of mild steel in hydrochloric acid solution, Journal of Molecular Liquids, 244 (2017) 154-168.

[41]A. Berisha, F.I. Podvorica, V. Mehmeti, F. Syla, D. Vataj, THEORETICAL AND EXPERIMENTAL STUDIES OF THE CORROSION BEHAVIOR OF SOME THIAZOLE DERIVATIVES TOWARD MILD STEEL IN SULFURIC ACID MEDIA, Macedonian Journal of Chemistry and Chemical Engineering, 34 (2015) 287-294.

[42]A. Popova, M. Christov, A. Zwetanova, Effect of the molecular structure on the inhibitor properties of azoles on mild steel corrosion in 1 M hydrochloric acid, Corrosion Science, 49 (200 (7 .2143-2131

[43]S. Erdogan, Z.S. Safi, S. Kaya, D.O. Isin, L. Guo, C. Kaya, A computational study on corrosion inhibition performances of novel quinoline derivatives against the corrosion of iron, Journal of Molecular Structure, 1134 (2017) 751-761.

[44]F. Benhiba, Z. Benzekri, A. Guenbour, M. Tabyaoui, A. Bellaouchou, S. Boukhris, H. Oudda, I. Warad, A. Zarrouk, Combined electronic/atomic level computational, surface (SEM/EDS), chemical and electrochemical studies of the mild steel surface by quinoxalines derivatives anti-corrosion properties in 1 mol.L-1 HCl solution, Chinese Journal of Chemical Engineering, 28 (2020) 1436-1458.

[45]H. Shokry, Molecular dynamics simulation and quantum chemical calculations for the adsorption of some Azo-azomethine derivatives on mild steel, Journal of Molecular Structure, 1060 (2014) 80-87.

[46]S.K. Saha, A. Dutta, P. Ghosh, D. Sukul, P. Banerjee, Adsorption and corrosion inhibition effect of Schiff base molecules on the mild steel surface in 1 M HCl medium: a combined experimental and theoretical approach, Physical Chemistry Chemical Physics, 17 (2015) 5679-5690.

[47]A. Dutta, S.K. Saha, U. Adhikari, P. Banerjee, D. Sukul, Effect of substitution on corrosion inhibition properties of 2-(substituted phenyl) benzimidazole derivatives on mild steel in 1 M HCl solution: A combined experimental and theoretical approach, Corrosion Science, 123 (2017) 256-266.

[48]L.H. Madkour, S. Kaya, L. Guo, C. Kaya, Quantum chemical calculations, molecular dynamic (MD) simulations and experimental studies of using some azo dyes as corrosion inhibitors for iron. Part 2: Bis-azo dye derivatives, Journal of Molecular Structure, 1163 (2018) 397-417.

[49]W. Yang, W.J. Mortier, THE USE OF GLOBAL AND LOCAL MOLECULAR-PARAMETERS FOR THE ANALYSIS OF THE GAS-PHASE BASICITY OF AMINES, Journal of the American Chemical Society, 108 (1986) 5708-5711.

[50]R.K. Gupta, M. Malviya, K.R. Ansari, H. Lgaz, D.S. Chauhan, M.A. Quraishi, Functionalized graphene oxide as a new generation corrosion inhibitor for industrial pickling process: DFT and

experimental approach, Materials Chemistry and Physics, 236 (2019).
[51]M. Messali, M. Larouj, H. Lgaz, N. Rezki, F.F. Al-Blewi, M.R. Aouad, A. Chaouiki, R. Salghi, I.M. Chung, A new schiff base derivative as an effective corrosion inhibitor for mild steel in acidic media: Experimental and computer simulations studies, Journal of Molecular Structure, 1168 (2018) 39-48.
[52]J.M. Roque, T. Pandiyan, J. Cruz, E. Garcia-Ochoa, DFT and electrochemical studies of tris(benzimidazole-2-ylmethyl)amine as an efficient corrosion inhibitor for carbon steel surface, Corrosion Science, 50 (2008) 614-624.
[53]H.L. Wang, X.Y. Wang, L. Wang, A.H. Liu, DFT study of new bipyrazole derivatives and their potential activity as corrosion inhibitors, Journal of Molecular Modeling, 13 (2007) 147-153.
[54]B. Gomez, N.V. Likhanova, M.A. Dominguez-Aguilar, R. Martinez-Palou, A. Vela, J.L. Gazquez, Quantum chemical study of the inhibitive properties of 2-pyridyl-azoles, Journal of Physical Chemistry B, 110 (2006) 8928-8934.
[55]A. Singh, K.R. Ansari, Y.H. Lin, M.A. Quraishi, H. Lgaz, I.M. Chung, Corrosion inhibition performance of imidazolidine derivatives for J55 pipeline steel in acidic oilfield formation water: Electrochemical, surface and theoretical studies, Journal of the Taiwan Institute of Chemical Engineers, 95 (2019) 341-356.
[56]S. Uzun, Z. Esen, E. Koc, N.C. Usta, M. Ceylan, Experimental and density functional theory (MEP, FMO, NLO, Fukui functions) and antibacterial activity studies on 2-amino-4-(4-nitrophenyl)-5,6-dihydrobenzo h quinoline-3-carbonitrile, Journal of Molecular Structure, 1178 (2019) 450-457.
[57]C. Morell, A. Grand, A. Toro-Labbe, New dual descriptor for chemical reactivity, Journal of Physical Chemistry A, 109 (2005) 205-212.
[58]J.J. Zhou, S.H. Chen, L. Zhang, Y.Y. Feng, H.Y. Zhai, Studies of protection of self-assembled films by 2-mercapto-5-methyl-1,3,4-thiadiazole on iron surface in 0.1 M H2SO4 solutions, Journal of Electroanalytical Chemistry, 612 -257 (2008) .268
[59]A. Kokalj, Comment on the A.B. Rocha's reply to second comment on the paper "On the nature of inhibition performance of imidazole on iron surface", Corrosion Science, 79 (2014) 215-220.
[60]E. a Badr, H.H. Hefni, S. Shafek, S.M.J.I.J.o.B.M. Shaban, Synthesis of anionic chitosan surfactant and application in silver nanoparticles preparation and corrosion inhibition of steel, (2020).
[61]S.M. Shaban, I. Aiad, F.A. Yassin, A.J.J.o.S. Mosalam, Detergents, The tail effect of some prepared cationic surfactants on silver nanoparticle preparation and their surface, thermodynamic parameters, and antimicrobial activity, 22 (2019) 1445-1460.